An Investigation of Nonlinear Flow Oscillations in a High-Pressure Centrifugal Pump

Claudio Lettieri[1]
MIT Gas Turbine Laboratory,
Massachusetts Institute of Technology,
Cambridge, MA 02139
e-mail: lettieri@mit.edu

Jeff Defoe[2]
MIT Gas Turbine Laboratory,
Massachusetts Institute of Technology,
Cambridge, MA 02139
e-mail: jdefoe@uwindsor.ca

Zoltán S. Spakovszky
MIT Gas Turbine Laboratory,
Massachusetts Institute of Technology,
Cambridge, MA 02139
e-mail: zolti@mit.edu

High-pressure multistage pumps and their coupled piping systems, typically used in the process and power generation industry, can experience dangerous system-level instabilities. This can occur at flow coefficients well away from the surge limit and in the absence of cavitation. Such a pumping system and a related new kind of instability are the focus of this paper. A system-wide instability was observed at 0.05 times rotor frequency for flow coefficients near maximum head rise but at negative slope, thus on the stable side of the head rise characteristic. A previous study based on system-level experiments concluded that this instability differs from classical surge, cavitation surge, rotating stall, and rotating cavitation, but the underlying mechanism and necessary flow conditions remain unknown. This paper investigates the root cause of the system-wide pump instability, employing a systematic analysis of the impact of geometry changes on pump stability and performance. It is found that the upstream influence of the unsteady flow separation in the return channel leads to a time-varying incidence angle change on the volute tongue which causes periodic ingestion of low-stagnation pressure fluid into the diffuser passages. This sets up a limit cycle, promoting the system-wide instability. With the instability mechanism determined, the pump is redesigned to remove the flow separation while maintaining performance at design conditions. Unsteady numerical simulations demonstrate improved efficiency and pressure recovery at low flow coefficients. A time accurate calculation also indicates stable operation at all relevant flow conditions. The paper resolves a long-standing pump stability problem and provides design guidelines for reliable and improved performance, important to the chemical processing and power generation industry. [DOI: 10.1115/1.4031250]

Introduction

A system instability was encountered in the high-pressure, multistage, centrifugal pump and piping network of a power plant. The instability is manifested as a large-amplitude system-wide oscillation at very low flow coefficients and below 25% of the pump's maximum efficiency point. At these conditions, the pump has a negatively sloped head rise characteristic, as shown in Fig. 1. The system instability occurs only when the resonant frequency of the piping network coincides with the unstable frequency range of the pump [1]. The frequency of oscillation is 4 Hz, which is lower than the frequencies typical for rotating cavitation. An experimental shop test of a two-stage representation of the ten-stage pumping system at increased inlet pressure showed the same unstable behavior, ruling out cavitation surge [1].

A large number of studies on cavitating and noncavitating pump instabilities, both experimental and theoretical, can be found in the literature. A widely used approach in modeling the dynamic behavior of a pumping system is the so-called transmission matrix method which relates the instantaneous changes in pressure and velocity at the inlet to those at the exit of the pump [2,3]. The approach describes the system impedance, which can be altered by cavities and their mass storage capability. The system-level behavior can then be represented in terms of mass gain factor and cavitation compliance. The determination of these coefficients, mostly from experiments, is challenging, especially for cases where the pump consists of multiple components of complex geometry. An attempt at a unified stability model for cavitating and noncavitating instabilities is presented in Tsujimoto et al. [4], where linearized one-dimensional and two-dimensional analyses are combined with a cavitating inducer actuator disk model, borrowing ideas from the classical Moore–Greitzer model for rotating stall and surge. More recently, the effect of downstream asymmetry in turbopumps, such as a volute, was also investigated, uncovering instabilities occurring at cavitation numbers above those generally observed during rotating cavitation and surge [5].

The pump under consideration in this paper operates at flow coefficients below 0.01 with regions of large separations and nonlinear behavior. An analysis of the isolated pump components suggests that the unstable behavior is governed by the coupling of

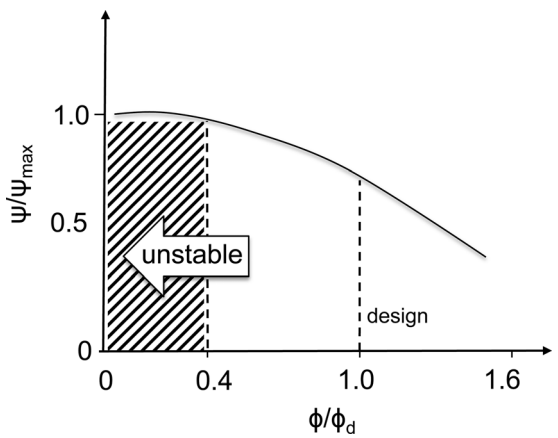

Fig. 1 Measured head rise characteristic of two-stage pump

[1]Corresponding author.
[2]Current position: Assistant Professor of Mechanical Engineering, University of Windsor, Windsor, ON N9B 3P4, Canada.

Contributed by the International Gas Turbine Institute (IGTI) of ASME for publication in the JOURNAL OF TURBOMACHINERY. Manuscript received November 12, 2014; final manuscript received August 4, 2015; published online September 2, 2015. Assoc. Editor: Stephen W. T. Spence.

the volute and deswirler. This behavior resembles that of inlet flow distortion effects in axial compressors on rotating stall and surge, in that the nonuniform mean flow, here induced upstream of the volute, alters the dynamic behavior and conditions for the onset of instability.

Guidelines for a design strategy to avoid this unstable behavior are not readily available. Makay [6] reported that instabilities might occur in pumps with a minimum flow coefficient higher than 25% of that for maximum efficiency. The root cause of this unstable behavior in pumps is not clear and remains a long-standing problem.

Volutes are often used in centrifugal pump designs because of their relatively simple geometry and reduced manufacturing costs. Volutes with a rectangular cross section are common in industrial applications [7] and are characterized by a constant-width flow path. The volute inlet width is obtained from the impeller outlet width b_2, the width of the impeller side-wall gaps, and the requirements of the casing design. The disadvantages are high inlet flow angles, radial and circumferential flow nonuniformities, and secondary flows, which develop during operation at off-design conditions. To increase the range of stable operation while maintaining pump performance, one design strategy is to use an impeller with a wider flow path and a vaned diffuser with reduced throat area, as outlined in Gulich [7], Casey et al. [8], and Lettieri et al. [9]. This approach increases the flow passage width at impeller exit, but reduces the width at diffuser inlet, effectively reducing the flow angle and potentially increasing the stable operating range. The best flow path width is chosen based on balancing requirements for performance and stability. Wider flow paths are beneficial for efficiency due to larger hydraulic diameters and reduced friction losses, but lead to high flow angles, which, at low flow coefficients, yield separation and instabilities.

Scope of Paper

This paper seeks to determine the physical mechanism that leads to the observed system-wide pump instability and aims to rigorously define a design strategy for stable operation at low flow coefficients. The work characterizes the root cause for a new type of noncavitating instability, different from classical surge and rotating stall. General guidelines are developed for the design of pumps with extended stability requirements.

The technical approach employs a systematic analysis of the effects of fluid dynamic component coupling on pump stability. It is found that the upstream influence of the separation in the volute diffusing passages leads to vortex shedding at the volute tongue, which couples with flow separation on the return vane, setting up a limit cycle. The instability due to the nonlinear interaction between the volute tongue, the volute diffusing passage, and the return vane separation can be inhibited by altering the feedback loop. This is investigated in a series of numerical experiments, isolating individual components contributing to the instability.

The volute and the deswirler, which consists of the return vane passages, are redesigned to remove the separation. The new design uses a vaned diffuser with a constant-width flow path. A rigorous parametric analysis defines the best flow path width to maintain performance while increasing the stable operating range. In this regard, a useful parameter to define the best flow path width is the ratio of the nondimensional impeller outlet width to the flow coefficient defined in Lettieri et al. [9]

$$b_2^* = (b_2/R)/\phi \tag{1}$$

which is directly related to the meridional velocity at the impeller exit, cm_2/U_T. Large values of b_2^* yield reduced meridional velocity in the passage, leading to reduced friction losses but increased flow angles. It will be shown that a vaned diffuser design with a nondimensional impeller exit width of $b_2^* = 10.5$ can maintain the pump efficiency at design within 0.5% and the head rise coefficient within 1.5% relative to the datum design. The redesign improves the pump efficiency and pressure rise at low flow coefficients by 10% and 2%, respectively, by keeping the flow attached throughout the diffuser and the return channel. Furthermore, unsteady analysis shows that the pump redesign is stable for all relevant flow coefficients, confirming the cause for unstable behavior being the separation in the volute.

The process used in the pump redesign follows that in Ref. [9], where the improvements of the stage redesign were demonstrated experimentally.

Numerical Methods

The computational method [10] is based on a finite volume approach using an implicit incompressible formulation with second-order spatial discretization. The Reynolds-averaged Navier–Stokes (RANS) equations are closed through the two-equation shear stress transport turbulence model. The mixing plane approach is employed between stationary and rotating components in the steady RANS computations while unsteady RANS simulations with a second-order backward-difference Euler approach using sliding interfaces are carried out to assess the pump stability. Unsteady calculations are used in the analysis of the isolated static components in Sec. 4, where the inlet flow profiles and dynamic behavior are taken from steady, single-stage calculations. These are also employed in the parametric study in Sec. 5. For all computations, the mass flow was specified at the outlet to set the desired flow coefficient.

The impact of mesh refinement on the normalized velocity profile at diffuser inlet is shown for the steady RANS in Fig. 2. Four different meshes were considered with y^+ varying from 20 down to 0.5. A baseline mesh was constructed following best practices for turbomachinery computational fluid dynamics (CFD) and was compared against a coarse mesh and two levels of mesh refinement. The total number of grid points for a single-passage calculation was approximately half a million for the coarse mesh, 1×10^6 for the baseline, 4×10^6 for the first refinement, and 7×10^6 for the second refinement. The wall roughness was set to an equivalent sand grain roughness of $0 \leq h_s^+ \leq 5$, representative of a highly polished smooth surface. The calculations suggest a maximum difference in velocity between the coarse and the baseline mesh of 2%. No appreciable difference in the velocity profiles of the baseline, first, and second refinements could be observed. Furthermore, the change in pressure rise and efficiency was less than 0.4% between the coarse and baseline meshes. Again there was no appreciable difference between the results for the baseline, the first refinement, and the second refinement. Therefore, all results in this paper are based on the calculations using the first mesh refinement.

Time-step sizes were determined based on best practices for second-order backward-difference methods [11,12]. A minimum

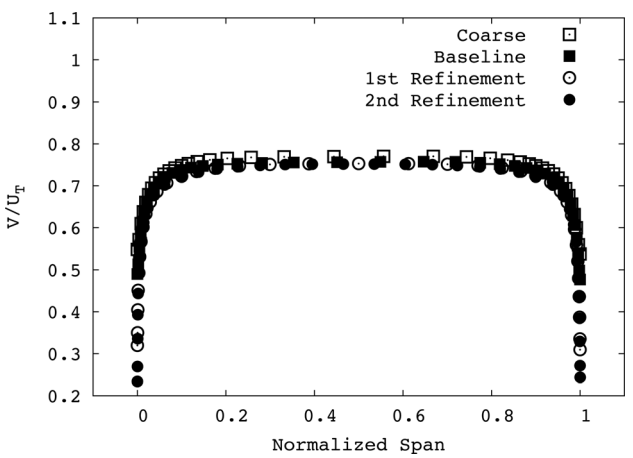

Fig. 2 Grid sensitivity analysis—velocity profiles at diffuser inlet for four meshes with increasing refinement levels

of 60 time-steps per period for the highest frequency of interest in each calculation was used.

The computational methodology used in this work has been successfully applied to other turbomachinery problems. The computations were experimentally validated for a liquid rocket turbopump inducer in water. The complex flow structure in the turbopump inducer is characterized by large regions of reversed flow [13]. Even so, the RANS computations predicted the total-to-static head rise coefficient to within 0.1% of experimentally determined values. A similar level of agreement with experimental data was demonstrated in a centrifugal pump operating with supercritical carbon dioxide [9]. The real gas computations at supercritical state and very high Reynolds numbers ($\sim 10 \times 10^6$) in the pump were within 0.2% of measured efficiency and pressure coefficient.

In summary, the numerical methodology used here has been extensively verified with experiments for a range of turbomachinery applications. Since new pump experiments were not planned within the time frame of the project, all performance and stability assessments in this paper are on relative basis.

Analysis of Datum Pump Design

A meridional view illustrating the pump geometry is shown in Fig. 3. The stage consists of a highly backswept shrouded impeller, a volute, and a deswirler. The volute collects the flow in discrete diffusing channels and directs it through the three-dimensional crossover bends into the return channels, each with a single return vane. The number of impeller blades was varied between three and four, the tip radius at the hub was reduced by 1.6% and the rotational speed varied from 1500 rpm up to 3000 rpm. These modifications did not alter the nature of the unsteady behavior, suggesting that the static components are the key to the pump stability. By investigating the detailed flow features in the static components through numerical simulations, the root cause of the instability is suggested to be self-sustained unsteady flow separations and vortex shedding from the volute tongue, in the diffusing passage, and on the return vane.

A total of three additional geometries, each isolating one of the components contributing to the feedback loop, were simulated for the datum stage to study the dynamic behavior. These are depicted in Fig. 4, together with the full stage (Sec. 4.1), a single passage of the static components (Sec. 4.2), and single passages with the return channel or vaneless space and tongue removed (Sec. 4.3).

For the full-stage case (geometry depicted in Figs. 3 and 4(*a*)), the static component dynamics are forced by the impeller wakes. These wakes can dominate the unsteadiness in the volute and deswirler, making it challenging to identify the unforced static component dynamic behavior. The unsteady flow behavior in the static components in the absence of any time-varying external forcing is therefore studied in detail.

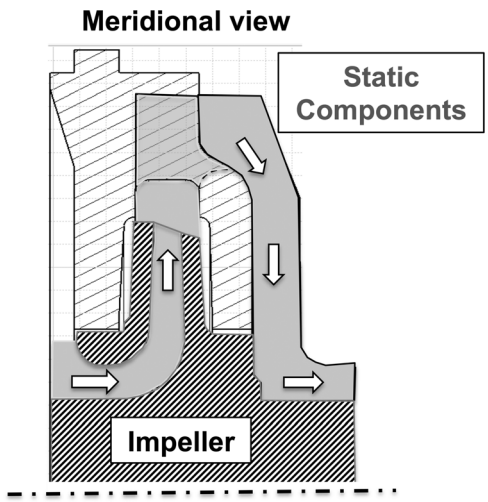

Fig. 3 Datum stage geometry

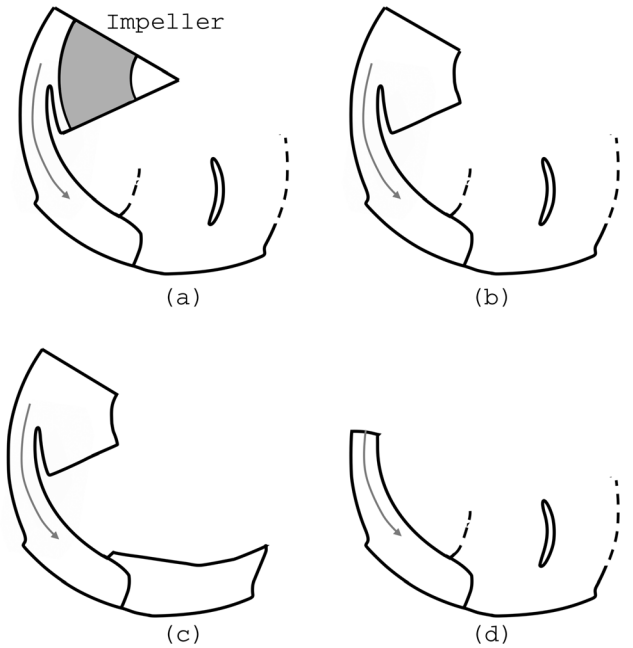

Fig. 4 Geometries used for datum stage calculations: (*a*) full stage, (*b*) single-passage, static components only, (*c*) single-passage, static components with return channel removed, and (*d*) single-passage, static components with vaneless space and volute tongue removed

Analysis of Full-Stage Flow Field

An initial full-stage analysis of the baseline configuration was conducted to characterize its performance and identify major flow features to be altered for improvement. The left side of Fig. 5 shows contours of normalized velocity in a blade-to-blade plane at 50% span, illustrating the flow field in a diffusing passage and return channel from calculations of the isolated static components. The flow behavior is identical to that from the full-stage calculation and shows three main features: a separation in the diffusing passage due to the area change, a large region of separation in the return channel due to the sharp 90 deg turn and large area change, and return vane separation and vortex shedding due to the flow underturning in the return channels caused by the upstream return channel separations.

One of the key contributors to the inefficiency of the multistage pump is the high amount of residual swirl at each stage's exit. The mass-averaged stage exit swirl angle at the design flow coefficient is greater than 40 deg. This is the result of the large region of flow recirculation in the return passages. The residual swirl is often hard to predict during the design phase and in addition to increased mixing losses, the inlet flow nonuniformity negatively impacts the performance of the downstream stage.

Datum Stage Without Impeller

To reduce the computational load, single-passage calculations were carried out. The flow interactions between the passages are weak because the design isolates the flow in each passage from diffusing passage inlet to return passage exit.

To assess the dynamic behavior of the static components, it is desirable to remove the effect of the impeller. This is because the magnitude of unsteady forcing imposed by the impeller wakes overwhelms the natural response of the static components in a full-stage computation. Therefore, calculations of the datum stage

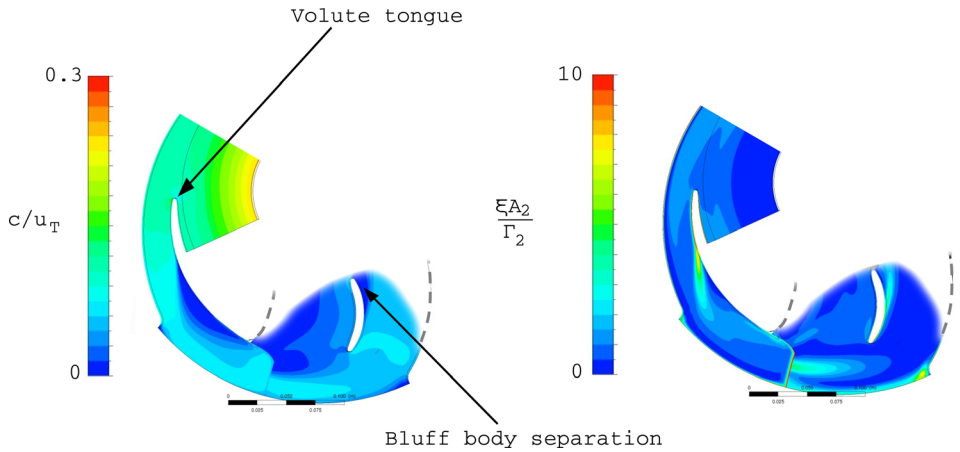

Fig. 5 Time-averaged flow field at midspan in static component calculation. Left: nondimensional velocity field and right: vorticity field. In each image, the portion to the left of the discontinuity is at midspan in the volute; the portion at right is at midspan in the deswirler.

without the impeller were performed for a single-passage computational domain. A radial inlet extension was added to prevent radially reversed flow at the inlet boundary. This inlet extension had inviscid walls to prevent boundary layer development and flow separation.

The flow coefficient of interest for the static component analysis was $\phi/\phi_d = 0.4$—the highest flow coefficient where system-level instability was observed. At this condition, the pitchwise-averaged flow angle at the impeller exit was 88.6 deg as determined by a steady, full-stage calculation. Regions of local backflow into the impeller are not accurately captured by the mixing plane between the impeller and diffuser, so that this flow angle is an estimate only.

When conducting the static component calculations, such high inlet flow angles did not allow the solver to converge. The highest attainable inlet flow angle was $\alpha_2 = 84.6$ deg and this was used throughout the analysis of the datum static components. Instability was observed with the reduced inlet flow angle, suggesting that there is uncertainty of at least ± 2 deg associated with the computed impeller outlet flow angle at $\phi/\phi_d = 0.4$.

Unsteady vortex shedding occurs in the diffusing passage and in the return passage. This sets up a limit cycle which promotes the system-level instability. The time-averaged flow field for the static components is depicted in Fig. 5. The same large regions of flow separation can be identified as in the full-wheel calculation, including in the diffusing passage and return channel, and from the trailing edge of the return vane.

The upstream influence of the bluff-body separation from the return vane contributes to the dynamic behavior of the flow in the entire stationary part of the stage by causing swings in incidence on the volute tongue. This results in periodic shedding and convection of low-stagnation pressure, vortical fluid from the suction side of the tongue into the adjacent diffusing passage as marked by the red arrow in Fig. 6. The drop in stagnation pressure for the suction side fluid of the volute tongue can be explained by examination of Fig. 7, in which the pathline through a point on the tongue suction side is shown. The long residence time in the vaneless space for these fluid particles, subject to shear from adjacent layers of fluid, leads to the stagnation pressure losses which promote separation of the diffusing passage boundary layer. In this simulation without the impeller, the recirculating pathlines extend to radii less than the impeller tip radius. However, the majority of the recirculation occurs in the vaneless space and near the impeller tip region. Therefore, the radial inlet extension is not expected to change the nature of the flow field behavior. If the impeller was present instead, these recirculating pathlines would be confined to the vaneless space. However, the long residence time in the vaneless space would likely still occur.

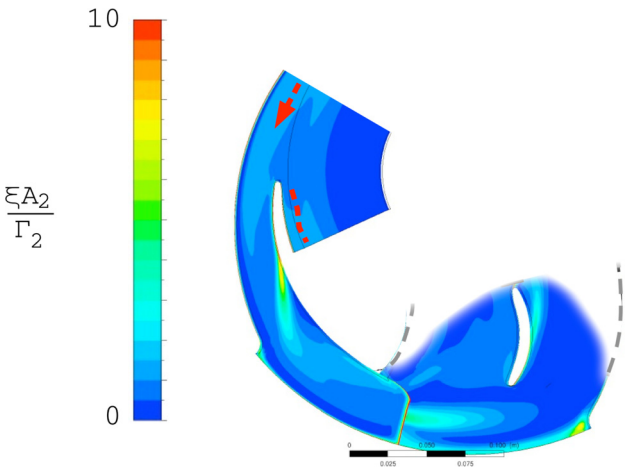

Fig. 6 Low-stagnation pressure fluid (red arrow) shed from volute tongue due to incidence swings enters adjacent diffusing passage

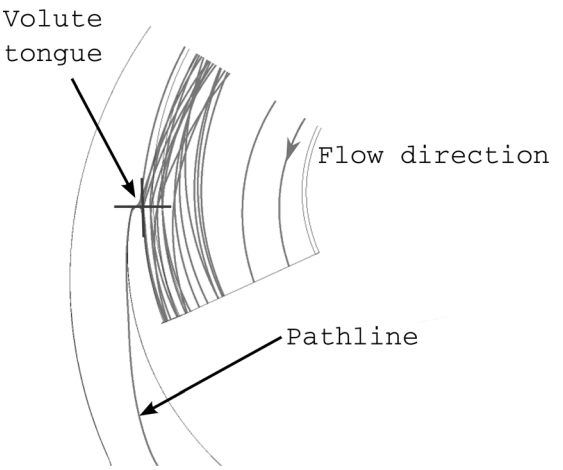

Fig. 7 Tongue boundary layer pathline, showing long residence time in the vaneless space. Pathline shown both upstream and downstream of the point indicated by the cross. Flow direction is counterclockwise as shown.

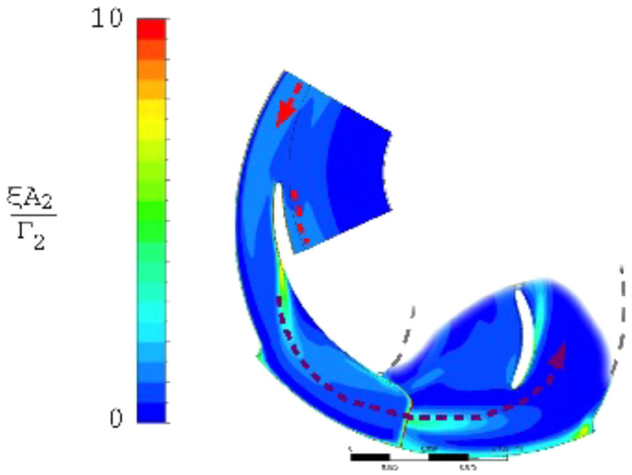

Fig. 8 Low-stagnation pressure fluid (red arrow) interacts with boundary layer in the diffusing passage, leading to vortex shedding (purple arrow). Shed vortices interact with the return vane, leading to bluff-body separation with upstream influence.

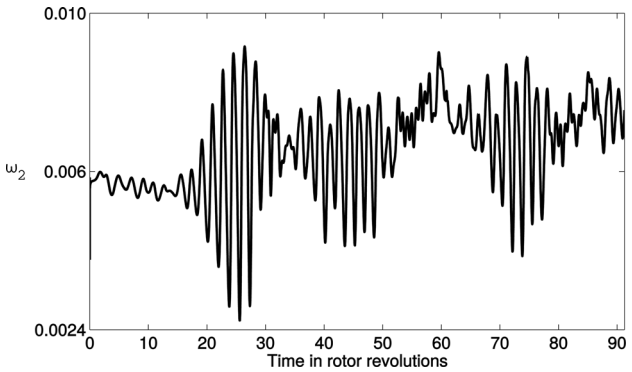

Fig. 9 Time trace of loss coefficient at stage exit, $\omega = (p_{t1} - \bar{p}_{t2}^{M})/0.5\rho U_T^2$

This fluid then interacts with the separated boundary layer in the diffusing passage, leading to vortex shedding. The shed vortices convect downstream (purple arrow in Fig. 8) and interact with the return vane, enhancing the vortex shedding there which gives rise to the upstream influence, thus closing the limit cycle.

In the initial transient phase of the unsteady calculation, oscillations begin as small perturbations and grow with time to nonlinear amplitudes until a limit cycle is established, as depicted by the time-trace of loss coefficient at stage exit in Fig. 9.

Determination of Components Required to Substain Limit Cycle

To corroborate the limit cycle hypothesis, a systematic study was conducted, removing individual static components to determine what conditions are required to sustain the feedback loop. Unsteady simulations were run without the return channel (Figs. 4(*c*) and 10(*b*)) and also without the upstream vaneless space and volute tongue (Figs. 4(*d*) and 10(*c*)). Removing the return channel has the effect of eliminating the upstream influence associated with the bluff-body separation from the return vane. Removing the vaneless space and tongue eliminates the periodically ingested slugs of low-stagnation pressure fluid into the diffusing passage. Removing the return channel involved adding an axial extension at the midpoint of the 180 deg bend as depicted in Fig. 10(*b*). This largely decouples the flow field within the volute from the downstream boundary condition. The axial extension has, by necessity, solid walls rather than the periodic boundaries found in the annular duct at stage exit when the return channel is present (Figs. 4(*b*) and 10(*a*)).

Removing the return channel completely eliminates vortex shedding in the diffusing passage, consistent with the limit cycle hypothesis. While there is still separation in the diffusing passage (as can be seen in Fig. 11(*b*)), no discrete vortices are shed.

The vaneless space was removed to investigate the effect of eliminating the periodic incidence angle variations on the volute tongue. The diffusing passage in this case receives a steady inlet stagnation pressure fluid and all unsteadiness in the flow field disappears. Some separations still exist (Fig. 11(*c*)), but without the periodic forcing imposed by a time-varying inlet stagnation pressure.

Mechanism for Feedback Loop

The analysis of the datum design static components shows that a feedback loop exists due to the interaction between several unsteady separations, which are conjectured to cause unstable operation of the entire pumping system. The feedback mechanism is identified as the upstream influence of bluff-body separation in the return channel. This upstream influence is manifested as a time-varying incidence angle on the volute tongue, leading to the periodic ingestion of low-stagnation pressure fluid into the diffusing passages.

Further analysis involving the removal of static components supports this explanation as the entire stationary geometry must be present for sustained unsteady separations to occur. If any stationary component is removed, the limit cycle behavior disappears.

One way to cut the feedback loop is to avoid separation in the volute, especially in the diffusing passages. This is the focus of the redesign effort with the goal of maintaining pump

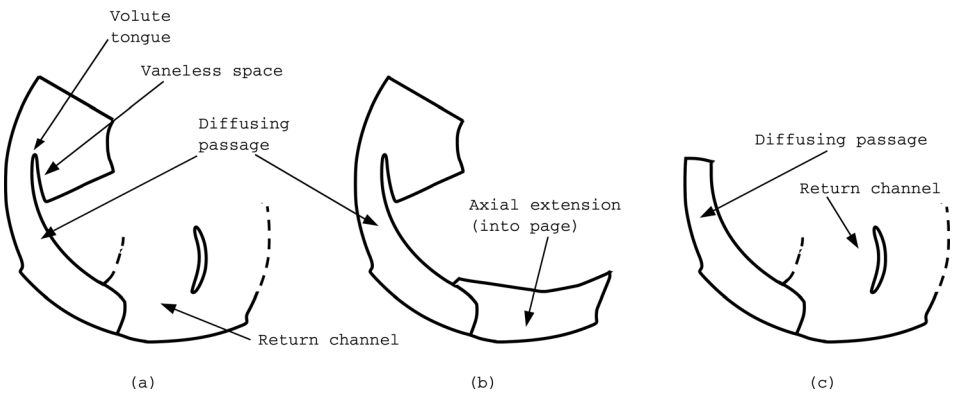

Fig. 10 (*a*) Single passage of static components, (*b*) static components with return channel removed, and (*c*) static components with vaneless space and volute tongue removed

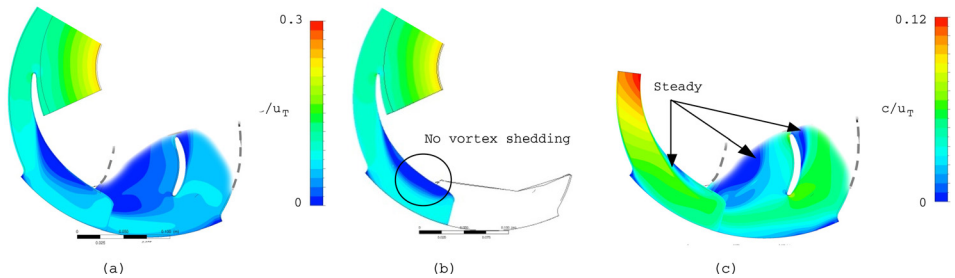

Fig. 11 Midspan velocity field: (*a*) all static components present, (*b*) return channel removed, and (*c*) vaneless space and volute tongue removed. Vortex shedding in the diffusing passage is inhibited when the return channel is removed. Vortex shedding is eliminated when the vaneless space and tongue are removed.

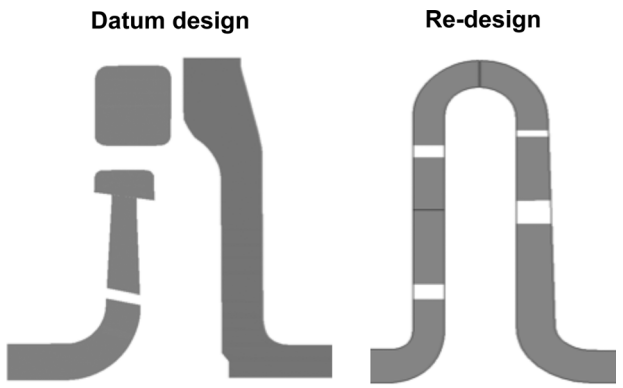

Fig. 12 Conventional flow path design with volute (left) versus new design with constant-width flow path and vaned diffuser (right)

performance at design flow coefficient while achieving stable operation at all relevant flow conditions.

Redesign Strategy to Cut Feedback Loop

Pumps with positively sloped characteristics near shut-off can also experience instability at flow coefficients for which the head rise curve is negatively sloped. One way to stabilize such pumps is to increase the recirculation at the impeller outlet by widening the flow path at impeller exit, as suggested in Gulich [7]. Other research on low flow coefficient pumps [8,9] suggests to reduce the throat area of the volute/diffuser and to make use of vaned diffusers so as to improve stability.

The redesign strategy therefore employs an impeller with increased outlet width and a vaned diffuser and return channel with constant flow path width, as shown in Fig. 12. Analysis of the flow field revealed that three-dimensional effects are not important in the range of operating conditions of the pump, with spanwise variations in blade loading below 0.1% at design conditions. To reduce manufacturing costs, the new components comprise prismatic, two-dimensional blades, and vanes. The narrower diffuser flow path reduces the diffuser throat area and decreases the inlet flow angle. The diffuser inlet blade metal angle is chosen to minimize incidence at low flow coefficients, trading performance at design for increased operating range. For the datum pump design, the wider flow path of the volute leads to a nearly tangential flow at the inlet to the return channel. In a multistage pump, it is desirable to remove the residual swirl before entering the next stage but the desire to achieve a compact geometry with reduced radius ratios makes deswirling without separation challenging. Therefore, the diffuser vanes are designed to reduce the swirl before entering the return channel, ultimately avoiding separation.

The impeller exit width is systematically increased in a parametric study to define the best flow path width minimizing the performance penalty while increasing the stable operating range. This is carried out using single-passage, steady CFD calculations of the isolated impeller. In this, a useful parameter is the nondimensional impeller width b_2^*, which is directly related to the flow coefficient at stage outlet as defined in Eq. (1). Typical high flow coefficient stages use a value between 1 and 1.5, and pump designs reported in Ref. [7] suggest that a value of 11 can be used. In the present study, this parameter was varied from a value of 9, representing the datum design, up to a value of 11. The design constraints that need to be met include the required work input coefficient, flow coefficient, and impeller rotational speed. It is important to note that the impeller outlet width and the blade outlet angle cannot be varied independently. In particular, a larger outlet width with a constant blade outlet angle will lead to an increased head coefficient. Assuming no swirl at the impeller inlet to maintain constant work input, the blade outlet angle was varied as shown schematically in Fig. 13 using one-dimensional analysis and the Wiesner slip correlation [14]. The effect of a larger b_2^* on the stage pressure recovery as well as the dependence of mass-averaged flow angle at the impeller exit on nondimensional impeller width is shown in Fig. 14.

In the assessment of the best choice of b_2^*, two competing effects must be taken into account. First, a wider flow passage reduces the meridional velocity at the impeller exit, lowering friction losses in the stage and increasing both the efficiency and the pressure recovery of the pump. Second, as the passage width is increased the flow becomes more tangential at the impeller exit, increasing the risk of radially reversed flow and reducing the stability margin of the diffuser.

Figure 14 shows that a nondimensional impeller width parameter of 10.5 leads to a more efficient pressure recovery at the impeller exit than in the datum design, yielding an increase of nearly 8% in total-to-total head rise coefficient with an diffuser inlet flow angle of approximately 82 deg. This analysis was conducted on a single-stage impeller configuration. The narrower diffuser removes the separation and reduces the inlet flow angle by approximately 4 deg compared to the datum design. A similar methodology for defining the best nondimensional impeller width parameter was adopted in the design of low flow coefficient supercritical carbon dioxide compressors [9] and validated experimentally, demonstrating an improvement in efficiency for a single stage of up to 3.5% points.

Performance and Stability Assessment of Redesigned Stage

A nondimensional impeller exit width of $b_2^* = 10.5$ is adopted in the stage redesign with a vaned diffuser. Three-dimensional, single-passage, steady CFD simulations were carried out to compare the performance with the datum design. In these simulations, leakage flows were consistently neglected to directly assess the

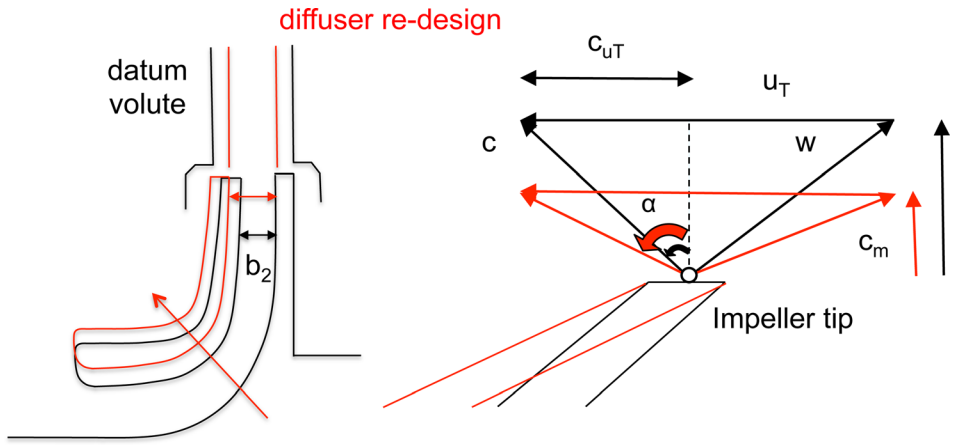

Fig. 13 To maintain fixed work input coefficient (and thus c_{uT}), the redesign with an increased, constant-width flow path leads to increased trailing edge blade angle and increase absolute flow angle at impeller exit

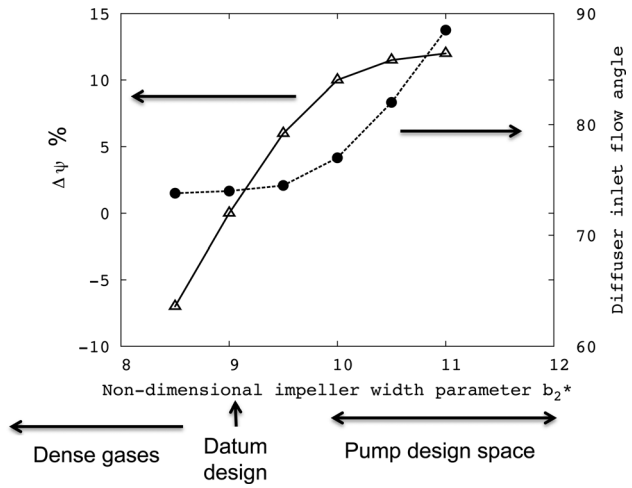

Fig. 14 Effect of b_2^* on mass-averaged diffuser inlet flow angle and total-to-total head rise coefficient

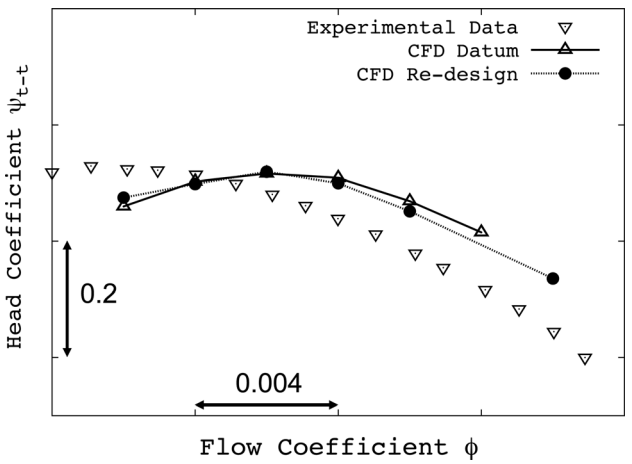

Fig. 15 Computed stage total-to-total head rise coefficient without leakage flow for original design and stage redesign. Experimental data (with leakage flows) are also shown.

impact of the stage redesign on the pump performance. The total-to-total head rise coefficient and total-to-total polytropic efficiency of the redesigned stage are compared with the original stage design in Figs. 15 and 16, respectively. Experimental data are also reported as a reference, but the data include the effects of the leakage flowpaths. The computed total-to-total head rise coefficient indicates that the redesign maintains pressure recovery to within 1.5% of the datum design at the design flow coefficient and increases the head rise by approximately 2% at 20% of the design flow coefficient. At high flow coefficients, the slope of the computed characteristic is similar to that in the experiment. However, the characteristic peaks at higher flow coefficient. At the lowest stable flow coefficient measured, the slope of the experimental pressure rise coefficient is close to zero whereas the computed characteristic is positively sloped. This is hypothesized to be due to the single passage assumption used in the calculations. Full-annulus unsteady computations of the datum pump demonstrate that flow blockage in one of the discrete passages leads to reduced incidence in the subsequent passage, decreasing the total flow blockage and increasing the overall head rise. In Fig. 16, the efficiency at design is reduced by 0.5% compared to that of the datum design. However, the redesigned stage yields up to a 10% improvement in efficiency at the lowest measured operating point. The analysis suggests that the redesign yields larger friction losses at the design flow coefficient, due to the higher velocity in the

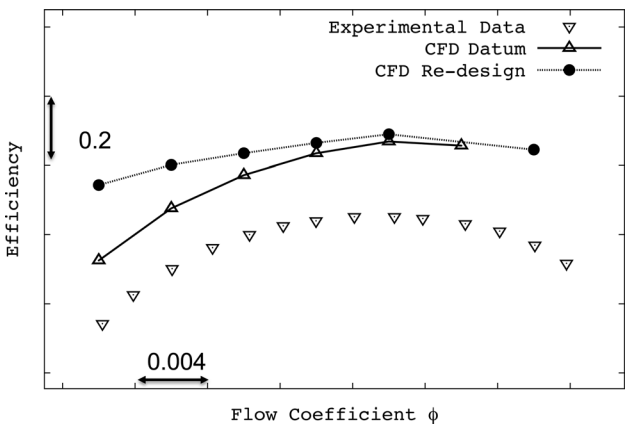

Fig. 16 Polytropic efficiency versus flow coefficient

diffuser caused by the reduced throat area. Although the redesign removes the flow separation in the diffuser and return channel, the effect on stage efficiency is much reduced at design flow coefficient due to the relatively low flow velocity in the pump. The separation losses in the datum design become more significant only at lower flow coefficients.

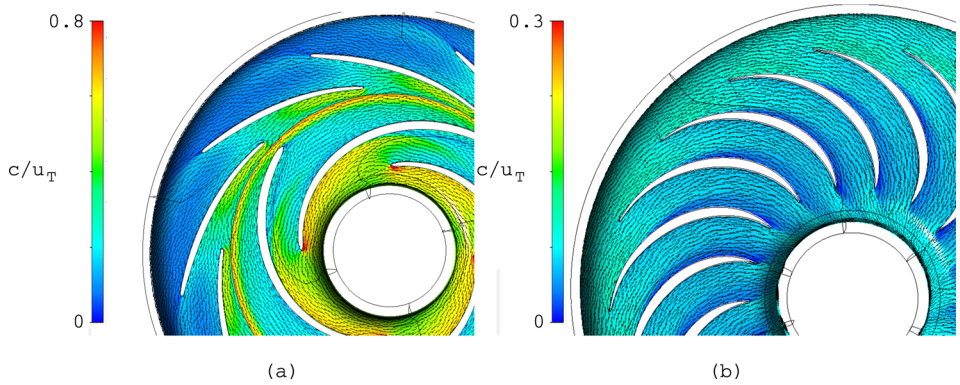

Fig. 17 Contour of normalized velocity at 50% span at the design flow coefficient of pump redesign. Velocities are relative in the rotating frame of the impeller and absolute for the stationary components. (*a*) Impeller and diffuser and (*b*) return channel.

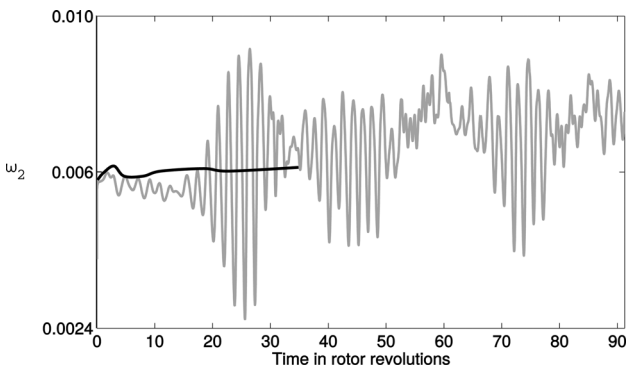

Fig. 18 Time trace of loss coefficient at stage exit, $\omega = p_{t1} - \bar{p}^{M}_{t2}/0.5\rho U_T^2$: black—redesign stage and gray—datum stage

From Figs. 15 and 16, it is also possible to assess the impact of the leakage flows. The computations overestimate the measured head rise coefficient by about 0.1. However, the slope of the characteristic is well-predicted, suggesting that the leakage flows have little impact on stage stability. The results further suggest that leakage flows yield an efficiency penalty of about 12% points.

Figure 17 depicts velocity contours in blade-to-blade planes at midspan. The velocities are relative for the rotating frame of reference of the impeller and stationary for the static components. The flow diffuses as it travel around the circumference at the impeller exit (shown as higher velocities in the rotating frame). The steady calculations indicate that flow separation is absent at the design flow coefficient. This is the case for all operating points down to 0.4 of the design flow coefficient, where a small separation and a reattachment is observed in the diffuser. The removal of the separations in the diffusing and return passages and the improved performance at low flow coefficients suggest stable operation. This is investigated next via a three-dimensional, full-annulus unsteady RANS calculation and compared with the results discussed in Sec. 4.

The time trace of the loss coefficient at stage exit is shown in Fig. 18 for both the redesigned stage (black) and the datum stage (gray) at 0.4 of the design flow coefficient, where instability was observed in the datum stage. The gray time trace is the same data shown in Fig. 9. The lack of sustained unsteadiness demonstrates that the redesign of the stage successfully cuts the feedback loop. Further analysis suggests an improvement of 20% in stable operating range.

Conclusions

Multistage pumps for power generation applications require stages with compact designs in both the radial and axial directions, high efficiency, and wide operating ranges. These pumps operate at flow coefficients below 0.01 for which the efficiency is much reduced due to dissipation in the flow path and increased leakage losses. Current design practice is to employ stages with wide flow paths and volutes to remedy the low performance. A common criterion for defining the stable operating range is based on the analysis of the pump head rise curve, where negatively sloped characteristics indicate stable operation. Centrifugal pumps with positively sloped characteristics toward shut-off have been found to experience instability for flow coefficients where the pump characteristic is negatively sloped [7]. Low-order models, such as transfer matrices, are often used to define the range of stable operation and to identify the unstable components. These methods, however, have limited accuracy and predictive capability for pumps with complex geometries and large regions of separated flow.

This paper investigated the instability of a pumping system with unstable behavior different from that of classical surge, rotating stall, cavitation surge, and rotating cavitation. The root cause of the instability was identified through systematic numerical assessment of the impact of geometry changes on stage stability. It is found that the unsteady separation in the stationary components of the pump leads to a feedback loop which promotes a nonlinear limit cycle as manifested, for example, in a large-amplitude oscillation of the stage loss coefficient.

The pump was redesigned to remove the separation so as to cut the feedback loop responsible for the unstable behavior. This redesign strategy has previously been applied to a supercritical carbon dioxide compressor and was experimentally verified [9]. To maintain the performance while improving the stable operating range, a pump impeller with a wider flow path and a vaned diffuser with reduced throat area were employed. The vaned diffuser was designed to turn the flow so as to reduce swirl before entering the return channel and to avoid flow separation. A parametric analysis was conducted to identify the best design in terms of nondimensional impeller width parameter. The simulations indicate that a stage with a nondimensional impeller width parameter of $b_2^* = 10.5$ maintains efficiency within 0.5% and pressure rise within 1.5% at design conditions, while increasing efficiency by 10% and pressure rise by 2% for the lowest stable operating point. Moreover, unsteady calculations suggest that the new stage design successfully cuts the feedback loop, yielding stable operation for flow coefficient as low as 20% of the design flow coefficient. Combined with the experimental findings in Refs. [9,13], the design approach and methodology presented here suggest to be

applicable to a wide range of centrifugal turbomachinery problems.

Nomenclature

A = area
b_2 = impeller width
b_2^* = $(b_2/R)/\phi$ nondimensional impeller width
c = absolute velocity
D = impeller diameter
h_s^+ = equivalent sand grain roughness
p = static pressure
p_t = stagnation pressure
R = impeller radius
U_T = impeller tip speed
w = relative velocity
y^+ = nondimensional wall distance
α = absolute flow angle
Γ = circulation
Δp = pressure rise
Δp_t = total pressure rise
ξ = vorticity
ρ = fluid density
$\phi = Q/D^2U_T$ flow coefficient
$\psi = \Delta p/0.5\rho U_{T^2}$ head rise coefficient
$\psi = \Delta p_t/0.5\rho U_{T^2}$ total-to-total head rise coefficient
$\omega = (p_{t1} - \bar{p}_{t^M}/0.5\rho U_T^2)$ loss coefficient

Subscripts

m = meridional component
u = circumferential component
x = axial component
1 = impeller inlet
2 = impeller outlet
θ = tangential component

References

[1] Kawata, Y., Ebara, K., Uehara, S., and Takata, T., 1987, "System Instability Caused by the Dynamic Behavior of a Centrifugal Pump at Partial Operation," JSME Int. J., **30**(260), pp. 271–278.
[2] Brennen, C., and Acosta, A., 1976, "The Dynamic Transfer Function for a Cavitating Inducer," ASME J. Fluids Eng., **98**(2), pp. 182–191.
[3] Greitzer, E., 1981, "The Stability of Pumping Systems: The 1980 Freeman Scholar Lecture," ASME J. Fluids Eng., **103**(2), pp. 193–248.
[4] Tsujimoto, Y., Kamijo, K., and Brennen, C., 2001, "Unified Treatment of Flow Instabilities of Turbomachines," AIAA J. Propul. Power, **17**(3), pp. 636–643.
[5] Brennen, C., 2007, "Multifrequency Instability of Cavitating Inducers," ASME J. Fluids Eng., **129**(6), pp. 732–736.
[6] Makay, E., 1978, "Survey of Feed Pump Outages, Research Project 641," EPRI, Report No. FP-754 4-2.
[7] Gulich, J. F., 2010, *Centrifugal Pumps*, Springer, London.
[8] Casey, M., Dalbert, P., and Schurter, E., 1990, "Radial Compressor Stages for Low Flow Coefficients," 4th European Congress on Fluid Machinery for Oil Petrochemical and Related Industries, The Hague, May 21–23, Vol. C403/004, pp. 117–126.
[9] Lettieri, C., Baltadjiev, N., Casey, M., and Spakovszky, Z., 2014, "Low-Flow-Coefficient Centrifugal Compressor Design for Supercritical CO_2," ASME J. Turbomach., **136**(8), p. 081009.
[10] ANSYS, 2012, "Academic Research Release 14.5, Theory Manual," ANSYS, Irvine CA.
[11] Defoe, J., Narkaj, A., and Spakovszky, Z., 2009, "A Novel MPT Noise Methodology for Highly-Integrated Propulsion Systems With Inlet Flow Distortion," AIAA Paper No. 2009-3366.
[12] Rumsey, C., Biedron, R., and Farassat, F., 1998, "Ducted-Fan Engine Acoustic Predictions Using a Navier–Stokes Code," J. Sound Vib., **213**(4), pp. 643–664.
[13] Brennen, C., 1994, *Hydrodynamics of Pumps*, Oxford University Press, Oxford, UK.
[14] Wiesner, F. J., 1967, "Review of Slip Factors for Centrifugal Impellers," ASME J. Eng. Gas Turbines Power, **89**(4), pp. 558–572.